

# New Ionization Hodoscope: design and characteristics

*V. Brekhovskikh<sup>a</sup>, M. Jabitski<sup>b</sup>, A. Kuptsov<sup>b</sup>, V. Lapshin<sup>a</sup>, V. Rykalin<sup>a</sup>, L. Tauscher<sup>c</sup>*

<sup>a</sup> *IHEP Protvino, Russia*

<sup>b</sup> *JINR Dubna, Russia*

<sup>c</sup> *Basel University, Switzerland*

## Abstract

In 2001 new forward  $dE/dx$  detector for the DIRAC experiment was constructed, calibrated and integrated into data analysis. Its design and characteristics are described in this note.

## Introduction

Pions, originated from pionium decay, are characterised by low relative momentum and cross upstream detectors at rather small relative distance. These atomic pairs cause double energy release by ionisation in a sensitive volume of the detector with respect to the ionisation loss by a single pion. Therefore, the uncertainties resulting from the inefficiency in detecting two tracks with relative distance approaching to zero can be significantly reduced.

The previous  $dE/dx$  detector consisted of 2 planes by 16 vertically oriented 2 mm thick scintillator slabs [1]. Therefore it could resolve close tracks only in one projection. It had geometrical inefficiency due to approximately 0.5 mm wide gaps between slabs. New Ionisation Hodoscope consists of 4 planes: two planes with vertically and two planes with horizontally oriented slabs. Adjacent slabs are separated by thinner gaps (about 60  $\mu\text{m}$ ). So it allows to distinguish close tracks in both projections with better acceptance.

We will demonstrate the feasibility of separation of double ionisation events from single ones with the help of the new  $dE/dx$  detector taking into account a system of corrections, which is different from [2].

## Design of the new Ionisation Hodoscope

The new Ionisation Hodoscope (IH) has been designed to eliminate the main drawbacks of the previous detector: absence of planes with horizontally oriented slabs and sizeable gap between adjacent slabs. The thickness of scintillation slabs have been chosen 1 mm to keep the same amount of scattering matter in the secondary particles channel. This leads to decrease of scintillation light from each slab. A few measures have been taken to get higher efficiency of the detector. Photomultipliers have been selected by the maximum quantum efficiency criteria from a large batch of FEU-85 photomultipliers. Scintillator BC-408 with high light output has been chosen as an active material for slabs. Photomultipliers have been connected to the wide side of a light guide instead of the traditional butt-end readout. This improves the light collection efficiency by about 50%.

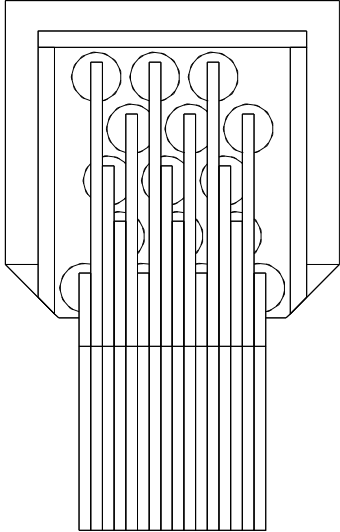


Figure 1: *Design of the scintillation plane.*

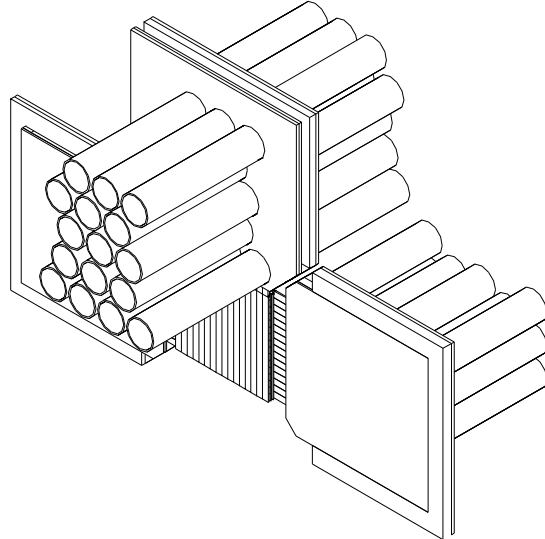


Figure 2: *Isometric view of the New Ionisation Hodoscope.*

The new Ionisation Hodoscope consists of 4 planes of  $11 \times 11 \text{ cm}^2$  in size placed normally to the axis of the setup, 3 metres downstream from the target and covers the full aperture of the secondary particles channel. Each plane is assembled from 16 plastic scintillator slabs made of fast scintillator (BC-408). Slabs are 11 cm long, 7 mm wide and 1 mm thick. They are connected to the PM photocathodes by 2 mm thick and 7 mm wide lucite (polymethylmethacrylate) light guides. As can be seen in figure 1 the light guides have different length. Small gaps between adjacent slabs was one of the main goals of the new detector. Each slab is wrapped by thin black mylar film ( $30 \mu\text{m}$ ) with an evaporated aluminium layer. The front surfaces of a slab are covered by a millipore film [3]. Light readout is done by FEU 85 PMs with  $\varnothing 25 \text{ mm}$  photocathode. Photomultipliers are arranged by 16 units into a compact set. This design allows independent replacement of each PM. Every plane of the Ionisation Detector can be quickly replaced, their relative position is adjusted by dedicated holes. As the detector is highly loaded by the flux of secondary particles, the last 4 dynodes have an additional power supply to ensure constant PM amplification throughout the spill.

The new Ionisation Hodoscope consists of 4 planes (see isometric view in figure 2). Two planes have vertically oriented slabs (so-called X-planes) and two planes are horizontally-oriented (Y-planes). They are arranged in the following order downstream of the secondary beam channel: XA-YA-XB-YB. Sometimes for conciseness we will refer to XA as plane A, to XB as B, to YA as C and to YB as D. This order of planes has been chosen to minimise possible cross-correlations between signals in planes (e.g. due to  $\delta$ -electrons). Planes with the same orientation of slabs are shifted by half of the slab width with respect to each other.

Both amplitude of a signal and its time are digitised by LeCroy ADC4300 and TDC3377. The principal scheme of the IH electronics is shown in figure 3. Note that the trigger logic was significantly simplified and amplitude integrators were excluded from the IH electronics. See [4] for details of the signal transfer and the trigger logic.

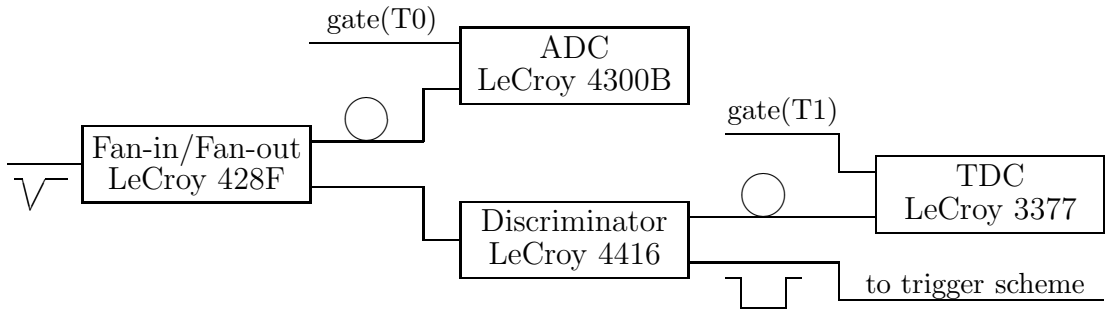


Figure 3: *The principal trigger scheme of the  $dE/dx$  detector.*

## Characteristics and calibration of the Ionisation Hodoscope

### ADC spectra

A typical ADC spectrum is shown in figure 4. On the horizontal axis amplitude  $A$  is represented:

$$A = \text{ADC}(\text{measured}) + \text{Online-pedestal-subtraction} - \text{Pedestal position}. \quad (1)$$

Note that  $A = 0$  corresponds to the "zero" of ADC. As ADC spectra have clearly seen structure with a period of 8 channels, for the further analysis all ADC spectra have been binned by 8 ADC channels per histogram bin. ADC spectrum collected with  $e^+e^-$ -trigger is presented in figure 5. Most electron-positron pairs have small opening angle and both particles cross the same slab of the Ionisation Hodoscope.

For conciseness we will refer to events with single and double energy release by ionisation as to single and double ionisation events. Tracks are reconstructed with the help of the offline DIRAC reconstruction program Ariane [5]. Events having only one reconstructed track in each arm of the spectrometer are selected. Each track must have one hit in Scintillation Fiber Detector (SFD) with time difference less than 4 ns from

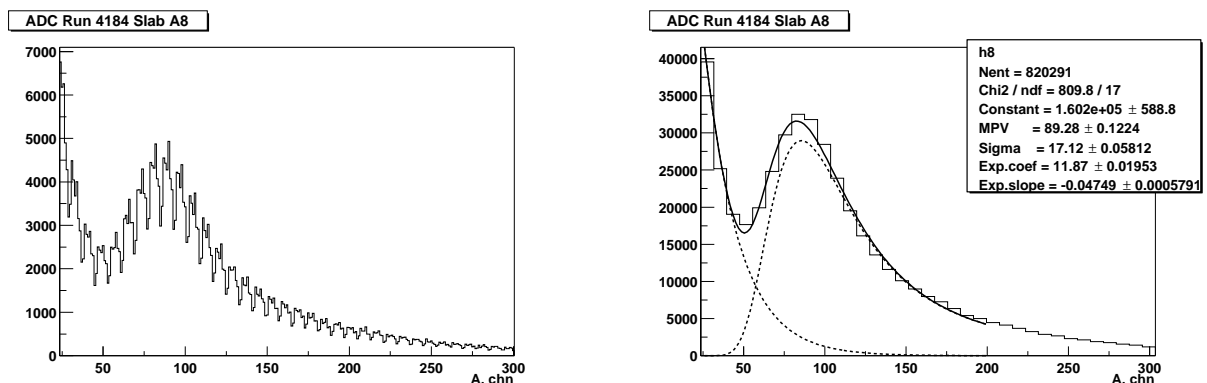


Figure 4: *Raw ADC spectra ( $\pi^+\pi^-$ -events): one ADC channel per bin (left), 8 ADC channels per bin (right). Histogram is fitted by a sum of the exponential and the Landau distribution, fit components are shown by dashed lines.*

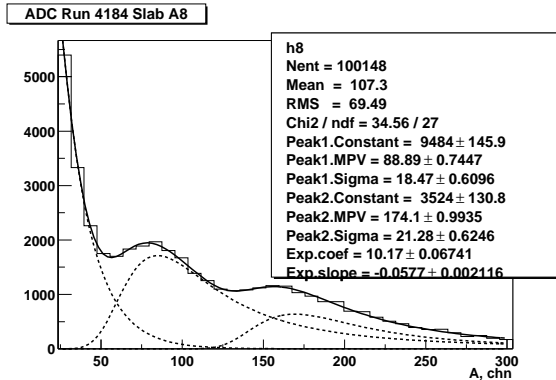


Figure 5: Raw ADC spectrum ( $e^+e^-$ -events).

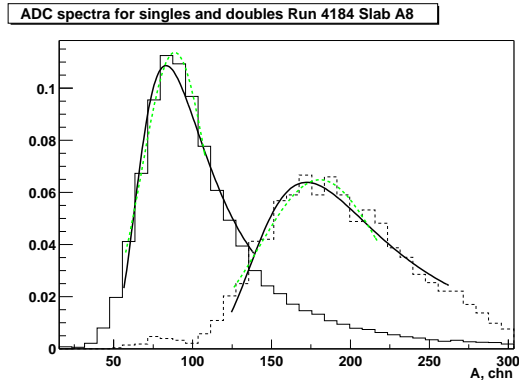


Figure 6: ADC spectra corresponding to events with single and double ionisation.

expected time, calculated from the time measured by Vertical Hodoscope (VH) and the pion time of flight. Additional cut, which requires no additional hits in SFD in the region  $\pm 20$  fibres around the fiber associated with a track, is applied. This cut implies absence of non-reconstructed tracks in the region of approximately 9 mm around the fiber hit by the particle. Track parameters allow us to reconstruct a point of intersection of the IH plane by the track and find a slab of the  $dE/dx$  detector corresponding to this track. In order to exclude possible uncertainties of the track reconstruction, for example due to multiple scattering, only tracks crossing the central part (90% of the slab width) of corresponding slabs have been selected. The ADC spectrum for selected events is shown in figure 6. If both tracks cross the central part of the same slab of the Ionisation Hodoscope they are associated with double ionisation events. Absence of background hits in the region  $\pm 20$  fibres around fibres hit by tracks is required. ADC spectrum corresponding to double ionisation is shown in figure 6 by dashed histogram.

The shape of single-particle ADC spectrum can be parametrised by Landau distribution of ionisation losses in a thin scintillator layer folded in with the appropriate Poisson statistics of photo-electrons on first dynodes. For detailed shape of ADC spectrum we refer to the following section "Simulation of the detector response" where the "close to reality" shape of the spectrum will be reproduced. It was found that the Landau shape provided by [6] rather well reproduces the main features of the measured distribution especially in the region around the peak. In order to estimate position of the peak fitting procedure is done in two steps. At the first stage experimental distribution is fitted by Landau distribution (solid curve in fig. 6). Then a fit by Gaussian distribution (dashed curve in fig. 6) is done in the region  $[\text{MPV} - 2\sigma_L, \text{MPV} + \sigma_L]$ , where MPV and  $\sigma_L^2$  are the most probable value and variance of the Landau fit. The mean value of the Gaussian curve is associated with the peak position. It's worth to note that in spite of the fact, that obtained mean value gives good approximation of the peak position, one has to pay special attention while attempting to describe shape of the experimental distribution (e.g. its width) in terms of parameters of the Gaussian fit.

## PM-ADC linearity

To estimate an amplification we introduce PM-ADC gain  $G$  — mean value of the ADC signal corresponding to the single minimum ionising particle (m.i.p.). If the detector gives the linear response to the energy lost by the traversing particle, zero of ADC ( $A = 0$ )

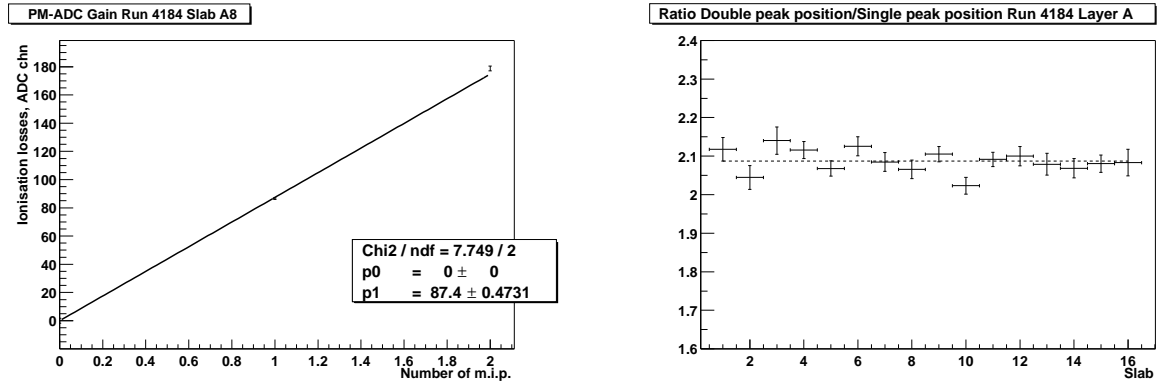


Figure 7: The left figure corresponds to a fit of PM-ADC gain by the linear function. The ratio of double and single ionisation peak positions computed for different slabs is presented in the right figure. Dashed line refers to the average of the ratio.

and both mean values of single and double ionisation peaks have to be points of one straight line (fig. 7). As the sample of double ionisation events is much less than single ionisation statistics, parameters of the fit are mainly defined by single-particle statistics. Ratio of mean values of single and double ionisation peaks is presented in figure 7. This ratio shows rather good linearity of the detector response and consistency of the described fitting procedure.

## Long term PM gain stability

The flux of secondary charged particles through the planes of the Ionisation Hodoscope is estimated to be more than  $10^7$  charged particles per beam spill ( $\approx 0.4$  s). This high flux leads to a typical rate of  $10^6$  hits per each slab and consequently to a high current through a photomultiplier. It was observed that the amplification of each photomultiplier decreases in time. The typical time dependence after a week without beam and without high voltage applied to PM is shown in figure 8. The most plausible explanation of the observed effect is the decrease of secondary emission coefficient for the last dynodes due to a high current through them. PM amplification partly recovers, if the high voltage has been switched off or there has been no irradiation for a few hours. This effect has been

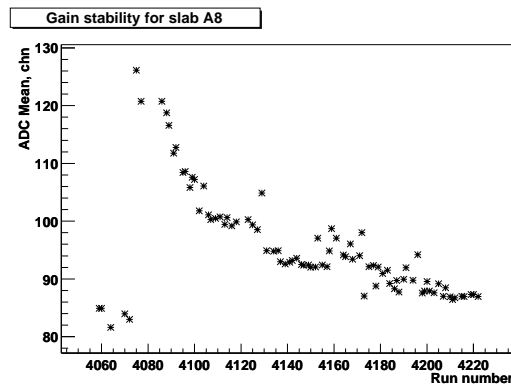


Figure 8: Gain stability as a function of time. Run 4075 was collected on 18/09/2001, run 4220 on 3/10/2001.

taken into account by calculating the gain for each run and applying the appropriate correction to the measured amplitude of the signal.

Note that the PM amplification factor decreases slowly in time and is nearly constant during one run. Nevertheless, just after the interruption the decrease during a run can be significant. As the set of corrections is prepared only for a whole run it is recommended to start data-taking for not so long runs just after the interruption.

## Reconstruction of slabs position

Figure 9 shows the coordinate map (X-map) of the detector: the distribution of tracks intersections with the first plane of the Ionisation Hodoscope which are correlated with signal in slab A8 are superimposed over the distribution of tracks intersections with the first plane of the Ionisation Hodoscope. The ratio of these distributions fitted with function

$$f(x) = \frac{p_0}{e^{-p_4(x-p_1)} + e^{p_4(x-p_2)}} + p_3 \quad (2)$$

provides the position of the slab. The precision of the intersection coordinate is mainly determined by the SFD granularity (0.44 mm). From fitting it was found that gaps between adjacent slabs are less than 0.1 mm. Dips around the slab in figure 9 are due to the algorithm of tracks selection, which requires no additional hits in SFD in the region around the fiber associated with the track.

The reconstructed layouts of scintillation slabs in X- and Y-planes of the new Ionisation Hodoscope are shown in figure 10 together with the local co-ordinate systems. Note that slabs in X-planes are numbered from left to right, slabs in Y-planes are numbered from bottom to top. Light from X-planes is readout from the top edge, light from Y-A plane — from left and light from Y-B plane — from right, if one looks downstream the secondary beam channel.

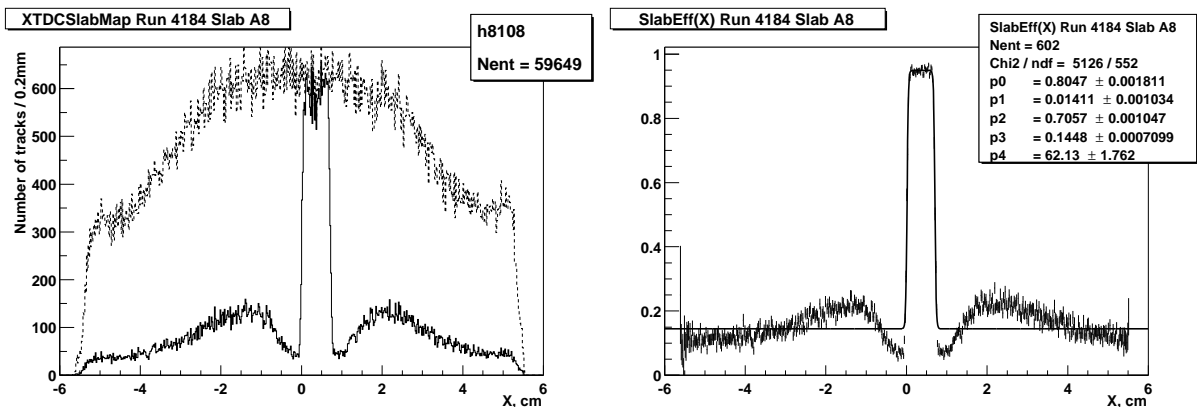


Figure 9: *The left figure: events with tracks correlated with hit in the slab A8 (solid line) are superimposed over X-map of tracks (dashed line). The right figure corresponds to the ratio of number of events correlated with hit in slab A8 over the total number of tracks (solid line is a fit by function 2).*

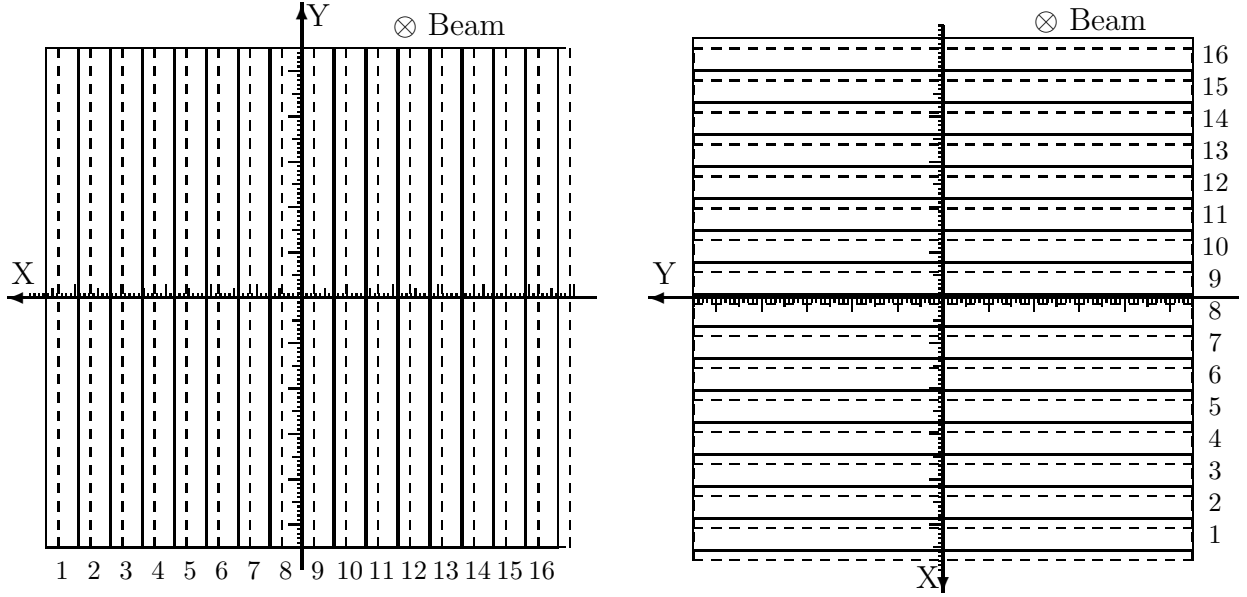


Figure 10: Reconstructed layouts of the X- and Y-planes of the IH. X-A and Y-A planes are shown by solid lines, X-B and Y-B planes are drawn by dashed lines.

## Amplitude longitudinal dependence

Knowledge of the detector amplitude response to the ionisation losses along the length of the scintillator slab is crucial for the correct separation of double ionisation events from single ones. The investigation was carried out on each slab by fitting the mean value of the ADC spectrum as a function of the particle impact onto the scintillator (fig. 11). A third order polynomial is sufficient to describe longitudinal dependence

$$A(y) = A(0) \cdot Y(y) = A(0) \cdot (1 + y(c_1 + y(c_2 + yc_3))). \quad (3)$$

The longitudinal dependence differs from slab to slab due to the different lengths of the light guides and due to the quality of each scintillator-light guide system. The signal from a track near the light guide is 1.1 ÷ 1.5 times higher than that from the distant edge. Only three slabs (namely Y-B1, Y-B3, Y-B6 in the fourth plane) have larger differences

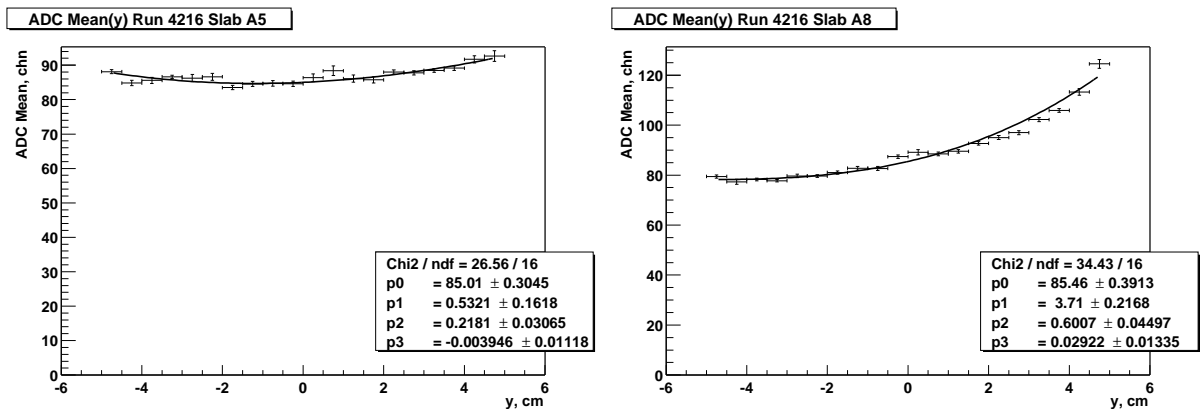


Figure 11: ADC longitudinal dependence for two slabs.  $p_i = p_0 c_i$ , ( $i = 1, 2, 3$ ) — polynomial coefficients.

probably due to assembling defects. Notice that in the previous Ionisation Hodoscope this factor was in the range  $1.4 \div 2.0$ .

The parametrisation of the longitudinal dependence in the form (3) explicitly separates the amplification  $A(0)$  from light collection. Thus  $Y(y)$  reflects only the longitudinal dependence of the light output from the scintillator-light-guide system and doesn't depend on the PM amplification. Consequently the set of coefficients in  $Y(y)$  is constant and valid during the whole period of data-taking with the same geometry of the detector. From experimental data it was found that the maximal variance in  $Y(y)$  defined for different runs doesn't exceed a few per cent even if the PM amplification changes up to a factor of two.

## Dependence of the measured amplitude on the time of signal with respect to the trigger

The significant dependence of the measured amplitude on the signal time with respect to the trigger was reported in 2000 [2]. For the data-taking with the new Ionisation Hodoscope the gate to its ADCs was increased to 70 ns. The gate starts with **T0** trigger, which requires coincidences in both arms of the spectrometer. It is delayed such that the start of the gate precedes the IH signal from triggered particles by approximately 20 ns [7]. Particles preceding or following the trigger by up to 20 ns are accepted. This still leads to some loss in the amplitude of the later signal, but not so dramatic as for the statistics of the year 2000 (fig. 12).

If there is only one track in each arm,  $\Delta t$  in figure 12 will be negative, unless there are some unreconstructed tracks or background hits which caused the trigger. In order to get events which came later and enrich region with  $\Delta t > 0$ , events having two reconstructed tracks in one arm and only one track in the other arm of the spectrometer were taken into account. Again all these tracks are propagated upstream the magnet and have corresponding different hits with proper timing in SFD. No other hits in the region  $\pm 20$  fibres around the fiber associated with a track are allowed.

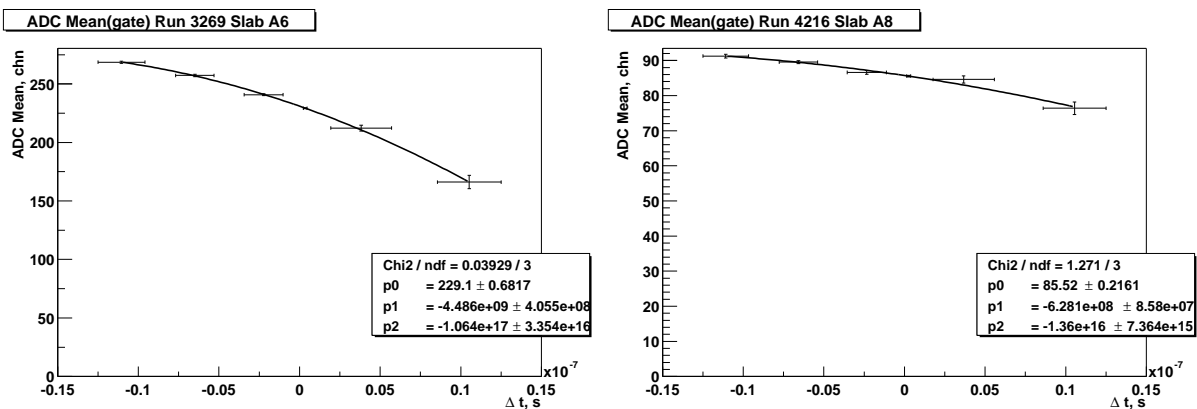


Figure 12: Mean ADC value dependence on the signal time with respect to the trigger.  $\Delta t$  — time difference between hit in the VH and **T0** time. The left figure corresponds to the data taken in 2001 with the old  $dE/dx$  detector (gate to ADC 56 ns), the right figure refers to the data taken in 2001 with the new  $dE/dx$  detector (gate to ADC 70 ns).  $p_i = p_0 c_i$ , ( $i = 1, 2$ ) — polynomial coefficients.



Time dependence of the ADC mean on the signal time is parametrised as

$$A(\Delta t) = A(0) \cdot T(\Delta t) = A(0) \cdot (1 + \Delta t(c_1 + \Delta t c_2)). \quad (4)$$

This parametrisation allows us to exclude part depending on the PM attenuation and to keep one set of corrections during the whole period of data-taking with the new  $dE/dx$  detector.

## Time delay dependence on signal amplitude

Time information from the  $dE/dx$  detector is used to verify correspondence between a reconstructed track and a hit in the Ionisation Hodoscope. The time of the hit corresponds to the moment when an amplitude of the signal exceeds the fixed threshold (fig. 13). Due to the difference in amplitudes of signals the measured time is shifted by a few nanoseconds (see fig. 14). Note that LeCroy TDC3377 modules work in the "COMMON STOP" mode. It means that the later signal corresponds to a smaller TDC count.

In figure 15 dependence of the TDC mean (obtained from the fit of the TDC distribution by Gaussian) on an amplitude of the signal is presented. It was fitted by the function

$$f(A) = -\exp(p_0 - p_1 A) + p_2. \quad (5)$$

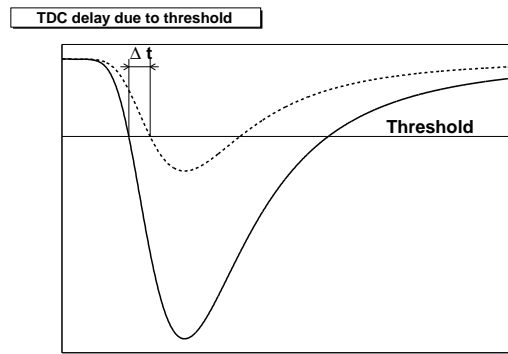


Figure 13: *Scheme explaining TDC delay due to a difference in amplitudes of signals.*

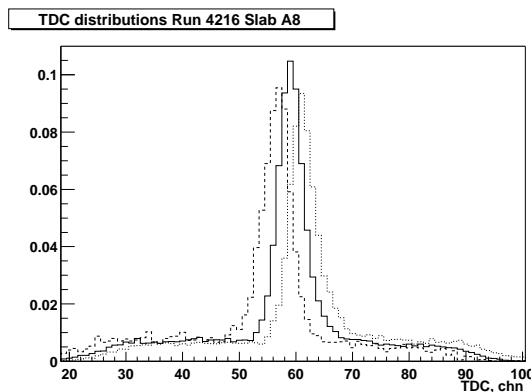


Figure 14: *TDC distributions for different ADC ranges:  $A < 60$  (dashed line),  $60 \leq A \leq 110$  (solid line) and  $A > 110$  (dotted line). One TDC channel is equal to 0.5 ns.*

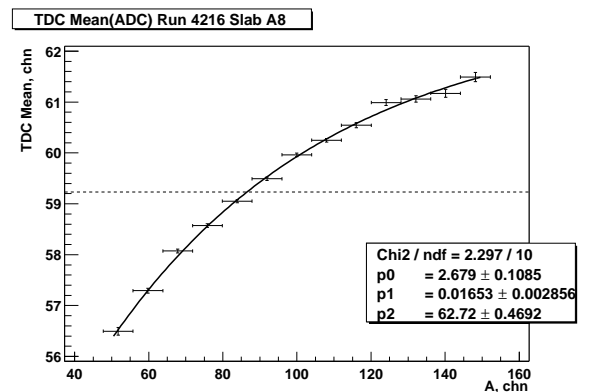


Figure 15: *TDC mean dependence on amplitude of the signal. Dashed line points to the TDC value corresponding to the ADC mean.*

Here the coefficient  $p_2$  reflects the constant shift of the TDC distribution with respect to the trigger time and has been already taken into account while calibrating the relative delay of the IH TDC time with respect to the VH timing. As the TDC mean  $\overline{\text{TDC}}$  with high accuracy coincides with  $f(\overline{A})$  one can express the additional time delay due to an amplitudes difference in the form

$$\Delta t = \left( -\exp(p_0 - p_1 A) + \exp(p_0 - p_1 \overline{A}) \right) \cdot C_{\text{TDC}}, \quad C_{\text{TDC}} = -0.5 \text{ ns}. \quad (6)$$

For reconstructed tracks one can estimate the expected time of a hit in the IH  $t_{\text{expected}}$  from the time of the hit in the Vertical Hodoscope and momentum of the particle. To estimate the time resolution of the  $dE/dx$  detector one can draw distributions of difference between  $t_{\text{expected}}$  and the time measurement by the Ionisation Hodoscope  $t_{\text{measured}}$ . Better resolution is obtained if one uses the timing corrected on signal amplitude  $t_{\text{corrected}}$  (see tab. 1). Note that the time resolution for  $\pi^+$  is worse than for  $\pi^-$  due to the admixture of protons into the spectrum of positively charged particles.

Table 1: Time resolution of the  $dE/dx$  detector.

	$e^+$	$e^-$	$\pi^+$	$\pi^-$
$\sigma(t_{\text{measured}} - t_{\text{expected}})$ , ns	1.05	1.00	1.33	1.09
$\sigma(t_{\text{corrected}} - t_{\text{expected}})$ , ns	0.83	0.78	1.14	0.91

## Other dependencies

As the scintillation light is read out only from one edge of a slab, it is expected that signal from a distant part of a slab is delayed with respect to a part close to a light guide. The dependence of the TDC mean on longitudinal co-ordinate is shown in figure 16. If correction 6 is applied, then difference between mean TDC values for different longitudinal co-ordinates doesn't exceed 0.7 ns ( $c_{\text{spread}} < 7 \text{ ns/m}$ ). This dependence on  $y$  practically doesn't affect the current data analyses, but can be taken into account if more precise time measurement by the IH will be required.

Due to the long term PM gain instability, the question, whether the PM amplification is stable during the spill duration, has been studied. It was found that the gain is stable enough throughout the spill (see fig. 17).

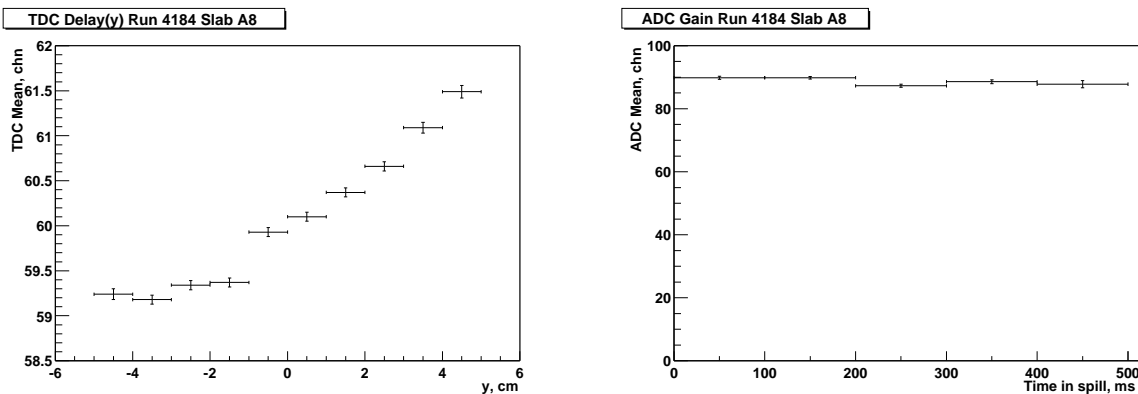


Figure 16: *TDC mean as a function of longitudinal co-ordinate.*

Figure 17: *Gain dependence on time during the spill.*

From the data analyses it was realised that the detector response to electrons is very close to the response to pions. No momentum dependence has been observed for pions from the kinematical region accepted by the setup.

## Corrections applied to the signal

Taking into account formulae (3) and (4) the measured ADC amplitude  $A$  can be expressed in the following form:

$$A(y, \Delta t) = A(0, 0) \cdot Y(y) \cdot T(\Delta t). \quad (7)$$

Note that applied corrections change the ADC mean. If the gain  $G$  for the corrected spectra is defined one can normalise  $A(0, 0)$  to it in order to exclude the long-term gain instability:

$$A_{\text{norm}} = \frac{100}{G} \cdot A(0, 0). \quad (8)$$

The later quantity doesn't depend on geometrical properties of the detector and features of the electronic scheme, thus it reflects the value of the energy release by ionisation by a traversing particle.

If both tracks cross the same slab of the Ionisation Hodoscope and are characterised by co-ordinates  $y_1, y_2$  with corresponding times  $\Delta t_1, \Delta t_2$ , the normalised amplitude  $A_{\text{norm}}$  can be estimated as the geometrical mean of two amplitudes

$$A_{\text{norm}} = \frac{100}{G} \cdot \frac{A}{\sqrt{Y(y_1)Y(y_2)T(\Delta t_1)T(\Delta t_2)}}. \quad (9)$$

## Singles/doubles separation

The quality of the separation of doubles from singles is crucial for the experiment. The single and double spectra after the normalisation are displayed in figure 18 together with curves derived from the spectra giving the fractional loss of double events and the

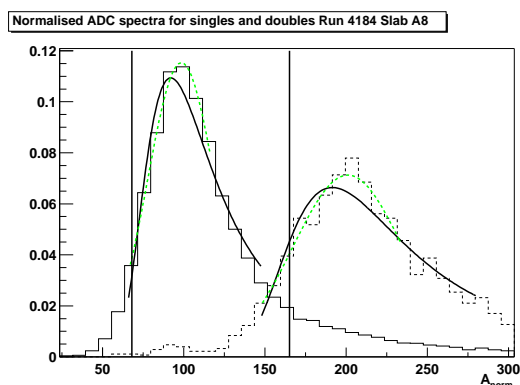


Figure 18: *Normalised ADC spectra for single and double ionisation. Vertical lines point to the single and double ionisation criteria.*

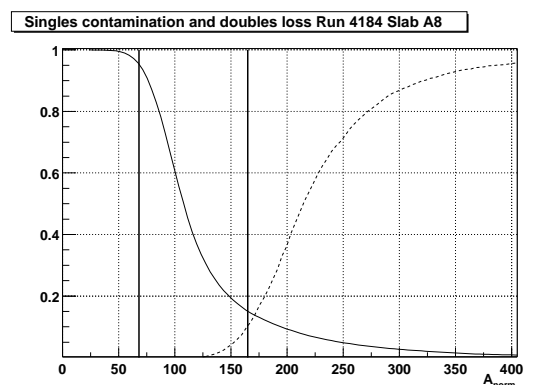


Figure 19: *Singles contamination and doubles loss (dashed line). Vertical lines correspond to the single and double ionisation criteria.*

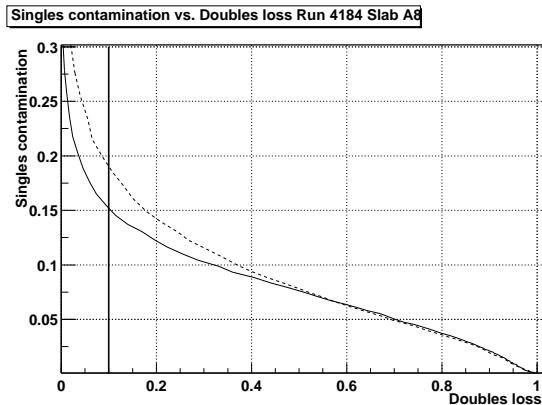


Figure 20: *Singles contamination versus doubles loss. Dashed line corresponds to singles/doubles separation without corrections applied. Vertical line shows proposed singles/doubles delimiter.*

fractional contamination of single events as a function of the normalised ADC amplitude (fig. 19).

In these figures proposed singles and doubles delimiters are shown. Singles criterion has been chosen for each slab such that 95% of single ionisation events are above it. It approximately coincides with the dip in the raw ADC spectrum (fig. 4). Position of the delimiter between single and double ionisation events can be chosen in different ways depending on how to keep contamination from singles small while cutting out as little as possible of double ionisation events. Here it corresponds to 10% loss of doubles, which leads to approximately 15% singles contamination (see fig. 20).

## Detector efficiency

Detector response to single tracks has been investigated to estimate detector efficiency. Detector efficiency for a slab is defined as a fraction of events which have signals corresponding to tracks intersecting this slab to the total number of events with tracks through this slab. Geometrical inefficiency due to gaps is estimated to be about 1% in each plane. One can easily see from figures 9 and 21 that uncertainties in the

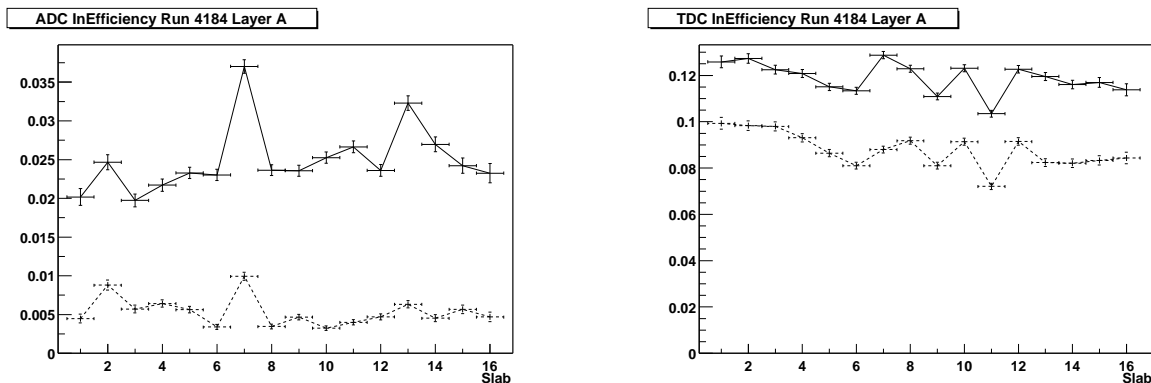


Figure 21: *Inefficiency of ADC (left) and TDC (right) responses to tracks crossing corresponding slabs (solid line) and to tracks crossing central part (80% of the width) of slabs (dashed line).*

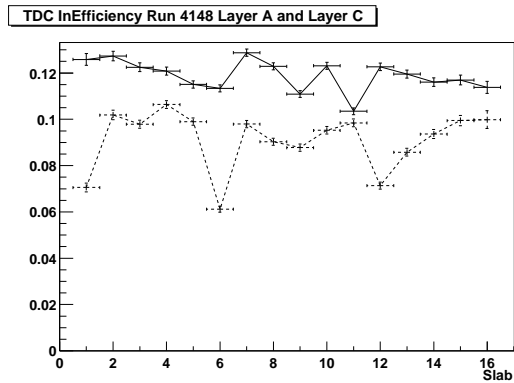


Figure 22: *TDC inefficiency for plane A (solid line) and plane C (dashed line).*

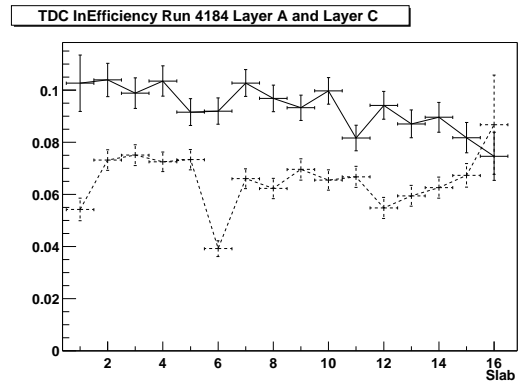


Figure 23: *TDC inefficiency for doubles: plane A (solid line) and plane C (dashed).*

track reconstruction increase the inefficiency. About 2 – 3% of reconstructed tracks are associated with a different slab they have actually crossed. So here the efficiency to find the slab corresponding to a track and the efficiency of the detector itself are combined into the term “detector efficiency”.

From figure 21 one can conclude that ADC inefficiency is mainly caused by the track–slab misfit. For TDC one requires not only the presence of the time measurement in the slab, in addition the measured time has to be inside of the  $\pm 4$  ns gate around the predicted time of the intersection of the slab by the track. TDC3377 can not correctly resolve hits which are closer then 20 ns. For this reason duration of the output logical signal from discriminator Le Croy 4416 (see fig. 3) was set to be longer than 20 ns. This duration calls forth the dead time in time measurement by the Ionisation Hodoscope. It was found that in 2001 the dead time for X-planes (70 ns) was longer than for Y-planes (35 ns) (fig. 22). In 2002 the dead time for all planes was reduced to 30 ns. Two signals which are so close in time result in a common ADC hit with an amplitude higher than the typical single particle amplitude (see fig. 24).

To get the TDC efficiency for events when two tracks have intersected the same slab of the Ionisation Hodoscope, the coincidence within 4 ns of the predicted time for the earliest track with the TDC time measurement is required. Inefficiencies for all slabs in first X- and Y-planes are presented in figure 23.

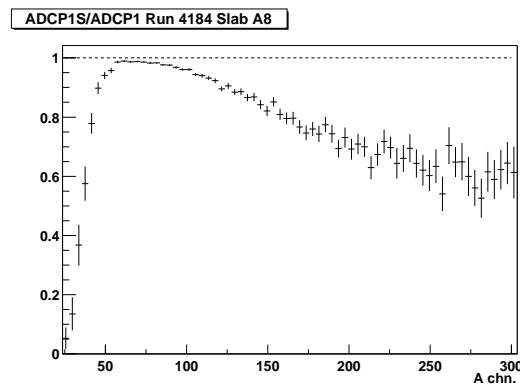
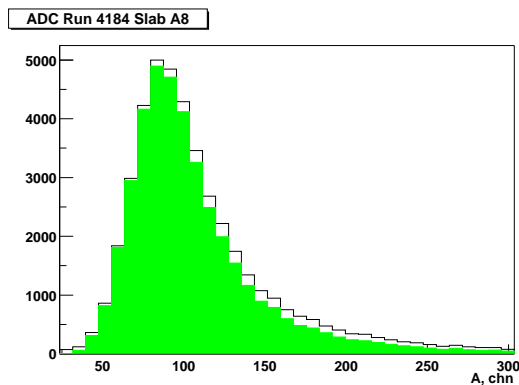


Figure 24: *In the left figure ADC spectrum (solid line) over ADC spectrum for events having proper time measurement by TDC (grey area) is shown. Right figure corresponds to the ratio of these ADC spectra.*

## Resolving the situation when two tracks have a common hit in SFD

The main purpose of the  $dE/dx$  detector is to resolve the uncertainties resulting from the inefficiency of SFD in detecting two tracks with relative distance approaching to zero. The subset of Ni 2001 data was analysed, events, when both downstream tracks were assigned with the same hit in SFD and there were no other hits in the region  $\pm 20$  fibres around it, were selected. This happens when two tracks have small relative momentum and have crossed upstream detectors at rather small relative distance. Another source of these events is an inefficiency of SFD. If one of the tracks has not been detected by SFD this track can be assigned by the reconstruction procedure with the hit from another track. Most of these background events can be rejected by applying the criteria of double ionisation in both planes of the Ionisation Hodoscope. In figure 25 clusters of singles and doubles are clearly seen.

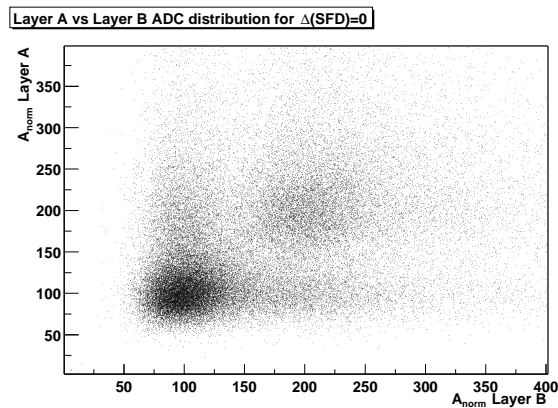


Figure 25: *Layer A vs. Layer B corrected ADC amplitudes  $A_{norm}$  for events with two tracks having a common hit in plane X of SFD. Ni target. Autumn 2001.*

Fractions of double ionisation in both planes of the  $dE/dx$  detector (D–D) and single ionisation in both planes (S–S) are presented in table 2. Only tracks with both ADC and TDC counts have been analysed. Mixed events which give single ionisation in one plane and double ionisation in another are coming mainly from long tails of the ADC distribution for singles.

The efficiency of the new Ionisation Hodoscope to analyse events with  $\Delta(\text{SFD}) = 0$  is about 75% and is mainly limited by the TDC dead time. The previous Ionisation Hodoscope had additional inefficiency of about 15% due to wider gaps between slabs,

Table 2:  $dE/dx$  efficiency to resolve  $\Delta(\text{SFD}) = 0$

	N. tracks	Can be analysed	S–S	Mixed	D–D
<i>New <math>dE/dx</math>:</i>					
Ni2001 (X planes)	75393	54608 (72%)	23139	14630	13271
Ni2001 (Y planes)	72537	55228 (76%)	19126	17182	15477
<i>Previous <math>dE/dx</math>:</i>					
Ti2001 (X planes)	124333	77409 (62%)	32999	20765	20682
Ti2001 (Y planes)		no planes			

which is much more than approximately 2% geometrical inefficiency of the new  $dE/dx$  detector. Events with two tracks assigned with one fibre of SFD are more than 30% in each projection in the kinematical region where atomic pairs from ponium decay are expected. Whether these events are coming from the pair of particles or artificially from inefficiency of SFD is difficult to decide unless the double criteria is applied in  $dE/dx$ . Thus information from the  $dE/dx$  detector allows us to recover significant part of statistics in the kinematical region where the atomic pairs are expected.

## Simulation of the detector response

For the GEANT-DIRAC [8] simulation program a code which reproduces typical amplitude and time distributions has been written. Distribution of ionisation losses by pion with momentum  $p = 2 \text{ GeV}/c$  in a scintillation slab is shown in figure 26. This distribution has been fitted by Landau distribution  $f = f(E)$ .

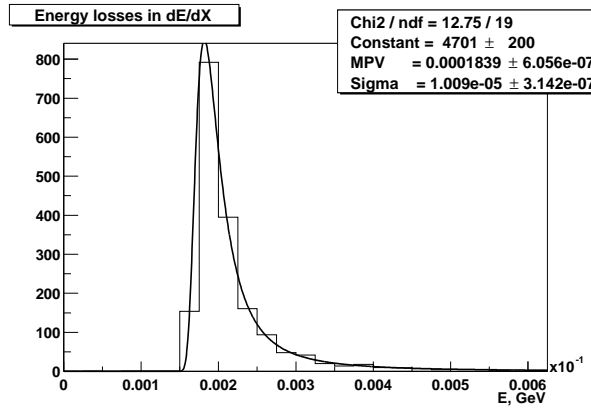


Figure 26: Ionisation losses by pion with  $p = 2 \text{ GeV}/c$  in the 1 mm thick scintillator (*Thanks to A. Benelli*).

If the distribution of ionisation losses  $f(E)$  is combined with the appropriate Poisson statistics of number of photo-electrons on the photocathode and first dynodes  $N$

$$w(N) = \frac{(\alpha E)^N e^{-\alpha E}}{N!}, \quad (10)$$

one can obtain an amplitude distribution measured by ADC:

$$A = A(E) = C \cdot N. \quad (11)$$

Here  $\alpha = N_{\text{p.e.}}(\text{MPV})/E_{\text{MPV}}$  is the ratio of the average number of photo-electrons  $N_{\text{p.e.}}(\text{MPV})$  to the most probable value of Landau distribution, which reflects a conversion efficiency of the detector.  $C$  is a scale factor converting PM response to ADC channels. The number of photo-electrons  $N_{\text{p.e.}}(\text{MPV})$  slightly varies between different PMs and is about 30 photo-electrons in DIRAC experimental conditions. The typical amplitude distribution combined with background hits is shown in figure 27.

Results of the separation of simulated single and double spectra are presented in figure 28, curves show separation for different numbers of photo-electrons  $N_{\text{p.e.}}(\text{MPV})$ .

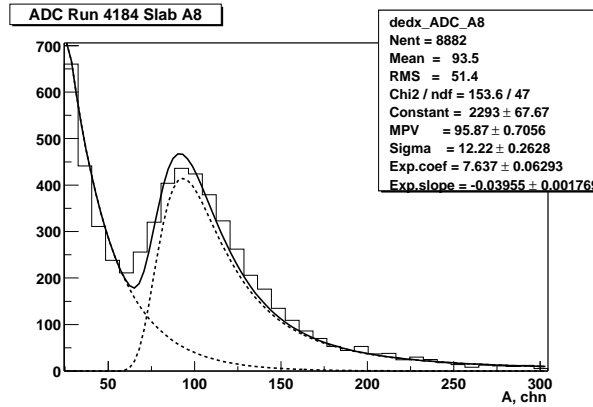


Figure 27: The simulated ADC spectra.

Note that curve  $N_{p.e.}(MPV) = 1000$  represents the possible lower limit of singles contamination to doubles for the 1mm thick plastic scintillator, because in this case the form of the simulated ADC spectra is defined only by the distribution of ionisation losses (see fig. 26). From figure 28 one can notice that simulation gives lower single contamination than it is experimentally observed (fig. 20). This reflects the fact that this simple simulation doesn't take into account many important processes, for example, background hits correlated with the track (e.g. by  $\delta$ -electrons) make the tail of singles spectra significantly higher. The spread of ionisation losses due to different energies of incident pions was not taken into account too.

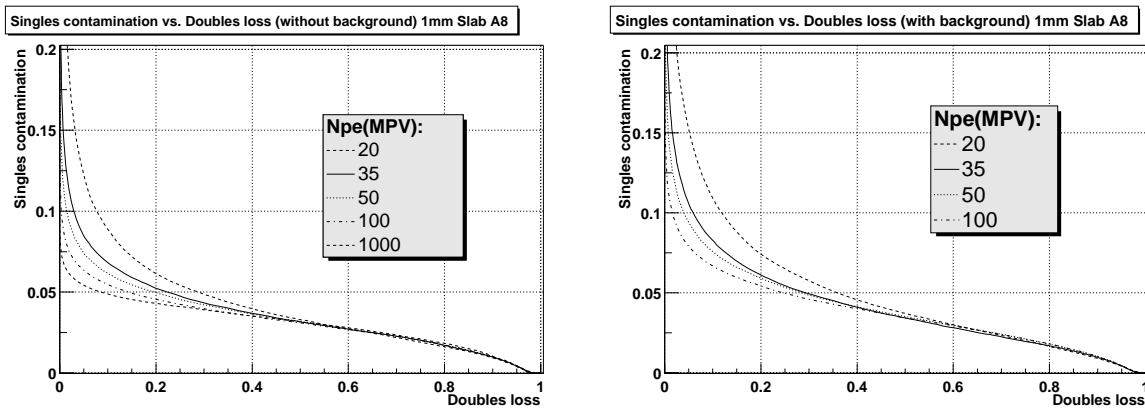


Figure 28: Separation of single and double spectra simulated without background (left) and with it (right) for different  $N_{p.e.}(MPV)$ .

## Ariane routines for the $dE/dx$ detector

Few subroutines which calculate corrections to amplitude and timing of signal from the IH have been added to Ariane. Note, that user have to set FFkey NoCorADCdEdX=2 in FFreadInput in order to initialise correct set of corrections.

```
real*4 function GetADCdEdXGainCorr(iHitdEdX)
```



This function returns normalised amplitude  $A_{\text{norm}}$  for the requested ADC hit `iHitdEdX`. Its output value is stored in variable `AmplHitDeDxGainCorr(iHitDeDx)` in COMMON BLOCK `IndEdX`.

```
real*4 function GetADCdEdXCorr(iHitdEdX,ytrdedx,timeVH,DelTime)
```

returns corrected normalised amplitude  $A_{\text{norm}}$  for the requested ADC hit `iHitdEdX`. `ytrdedx` is a longitudinal coordinate of the track in the local system of reference of the IH plane, `timeVH` — time of the hit in VH, `DelTime` is not used (for compatibility reasons). User can confront the obtained value of the corrected normalised amplitude  $A_{\text{norm}}$  with proposed values of single and double delimiters, which are stored in array `CritAmplDeDx` from COMMON BLOCK `DecTbldEdX`.

```
real*4 function GetTDCdEdXCorr(iHitdEdX,iTimEdX,ytrdedx)
```

returns corrected time of the hit in the  $dE/dx$  detector for the track, which is associated with ADC hit `iHitdEdX` and TDC hit `iTimEdX`, `ytrdedx` is a longitudinal coordinate of the track in the local system of reference.

## Conclusions

The new  $dE/dx$  detector has proven to be able to discriminate singles from doubles in both projections rather efficiently in DIRAC experimental conditions. The new Ionisation Hodoscope has low geometrical inefficiency due to thin gaps between adjacent slabs, which is about 2% in each projection. This value is much less than geometrical inefficiency of the old  $dE/dx$  detector, which was about 15% due to wider gaps. The presence of Y-planes gives a possibility to analyse a sample of data with  $\Delta(\text{SFD}(Y)) = 0$  which is estimated to be as large as 30% in the kinematical region where atomic pairs from ponium decay are expected. The system of calibrations has been developed and applied to data taken with both new and old Ionisation Hodoscopes. It allows us to incorporate the new  $dE/dx$  detector to the analysis of data taken by the DIRAC spectrometer and facilitates the pair identification by the experimental setup.

## Acknowledgements

The creation of the new  $dE/dx$  detector would not have been possible without the support of a great many people. Authors are indebted to A. Kulikov, V. Karpukhin and L. Afanasyev for their help with the implementation of the new IH to the trigger scheme. We wish to acknowledge V. Yazkov for a lot of useful discussions about details of tracking and data analysis. D. Drijard made a great work to incorporate set of corrections into Ariane. We would like to thank L. Nemenov for his permanent interest and support in the creation and implementation of the new  $dE/dx$  detector. Authors wish to acknowledge other members of DIRAC collaboration who helped us and had patience in different stages of this work.

## References

- [1] C. Detraz, D. Drijard, M. Ferro-Luzzi and V. Komarov, *The Ionisation Hodoscope: performance and characteristics of the first module*, DIRAC note 97-09.
- [2] A. Lopez-Aguera, *Ionisation detector offline alignment for Ni 2000 data taking*, DIRAC note 2001-03.
- [3] *Millipore* paper type HAWP pore size 0.45 made by MILLIPORE Corp., Bedford, Ma 01730 USA.
- [4] A. Kulikov, *Schematics of DIRAC trigger and readout electronics*, DIRAC note 2000-12.
- [5] D. Drijard, M. Hansroul, V. Yazkov, *DIRAC offline reconstruction program Ariane*, [www.cern.ch/dirac](http://www.cern.ch/dirac).
- [6] K.S. Kölbig and B. Schorr, *A program package for the Landau distribution*, Computer Phys. Comm. **31** (1984) 97–111.
- [7] A. Kulikov, *Private communication*.
- [8] P. Zrelov, V. Yazkov, *The GEANT-DIRAC simulation program*, [www.cern.ch/dirac](http://www.cern.ch/dirac).